Holocene fire regimes across the Altai-Sayan Mountains and adjacent plains: interaction with climate and vegetation types

Dongliang Zhang[1,2,3,*], Blyakharchuk Tatiana[4], Aizhi Sun[5,*], Xiaozhong Huang[6], Yuejing Li[1,2,3]

[1] *State Key Laboratory of Ecological Safety and Sustainable Development in Arid Lands, Xinjiang Institute of Ecology and Geography, Chinese Academy of Sciences, 818 Beijing South Road, Urumqi, China.*

[2] *Research Center for Ecology and Environment of Central Asia, Chinese Academy of Sciences, 818 Beijing South Road, Urumqi, China.*

[3] *University of Chinese Academy of Sciences, 19A Yuquan Road, Beijing, China.*

[4] *Institute of Monitoring of Climatic and Ecological Systems, Siberian Branch of Russian Academy of Sciences, Tomsk, Russia.*

[5] *College of Earth and Planetary Sciences, University of Chinese Academy of Sciences, Beijing, China.*

[6] *College of Earth and Environmental Sciences, Lanzhou University, Lanzhou, China.*

* Corresponding authors.

E-mail addresses: zhdl@ms.xjb.ac.cn and aizhisun@ucas.ac.cn.

Abstract: The Altai-Sayan Mountains and adjacent plains (including the west Siberian Plain, Kazakhstan Hills and Junggar Basin) have experienced accelerated warming in recent decades, raising growing concerns about escalating wildfire risks. However, two key gaps hinder understanding: paleofire dynamics in western Mongolia are understudied and no comprehensive regional synthesis exists for charcoal influx across the Altai-Sayan ecoregion. To address this, we reconstructed the Holocene fire sequence in western Mongolia and analyzed the spatiotemporal variations in charcoal influx across different vegetation zones of the Altai-Sayan Mountains and adjacent plains, as well as their coupling relationships with vegetation structure. The results reveal that Holocene declines in charcoal influx were driven by distinct mechanisms across subregions: above the forest limit in the central Altai Mountains, the decline was primarily controlled by temperature-limited woody biomass availability; in the western Sayan Mountains, it stemmed from the substantial expansion of fire-resistant *P. sylvestris*. Since ~2 cal. kyr BP, intensified anthropogenic disturbances—pecifically agricultural expansion and pastoral activities — have significantly increased fire frequency in the southeastern, western and northern Altai Mountains, the west Siberian Plain and the forest zones of central Altai Mountains. Conversely, the marked decline in charcoal influx observed in the

Khangai Mountains may be closely associated with vegetation fragmentation caused by overgrazing. Our findings provide a long-term perspective on fire-vegetation-climate interactions, offering critical insights for sustainable land management in the Altai-Sayan ecoregion.

Key words: Charcoal influx; Fire activities; Vegetation; Altai-Sayan Mountains

1. Introduction

The North Europe-Siberia-Altai region is the core distribution area of boreal forest ecosystems, hosting over 90% of the continent's boreal forest biomass and terrestrial organic carbon stocks (Furyaev, 1996; Kasischke, 2000). Its dynamics are closely intertwined with global climate system, forming a critical positive feedback loop. In 2021, wildfires in the global boreal forests released 1.76 $PgCO_2$, setting a historical record at that time (Zheng et al., 2023). Notably, the majority of carbon emissions from boreal forests originated from northern Eurasia. Carbon sequestration gain from a prolonged growing season may not offset carbon loss caused by enhanced respiration and disturbances (Mo et al., 2023). This ecological transformation triggers critical climate feedback mechanisms through carbon pool transformation, cascading ecological and permafrost degradation (Ivanova et al., 2019; Jones et al., 2020). This shift not only threatens regional carbon balance but also significantly accelerates global warming by releasing massive amounts of greenhouse gases, underscoring the extreme urgency of protecting this ecosystem for stabilizing the global climate.

Within this crucial northern Eurasian context, the Altai-Sayan region lies at the junction of Arid Central Asia and the boreal forest ecosystems. This region features an extremely steep hydrothermal gradient ranging from warm, arid steppes/shrublands in the south to cold, humid closed-canopy boreal forests in the north, forming a vast and sensitive ecotone (Xinjiang Comprehensive Investigation Team, CAS, 1978). It is precisely this "marginal" and "transitional" nature that makes it a natural laboratory and early warning system for studying fire-climate interactions (Fu et al., 2013; Liu et al., 2021). The convergence of two key flammability drivers–coniferous vegetation (*Pinus sibirica* dominance >60%) and intensifying drought regimes has created a

pyrogeographic hotspot. This synergy amplifies fire return intervals by 2.3× compared to pre-1990 baselines, fundamentally altering successional pathways and threatening ecological security thresholds (Goldammer & Furyaev, 2013).

Remote sensing analyses document a quadrupling of fire events from 712 ± 89 yr^{-1} (1980-2000) to 3024 ± 214 yr^{-1} (2001-2020) with burned area expanding exponentially ($R^2 = 0.91$, $p < 0.001$) (Ponomarev & Kharuk, 2016), which has a phase coincidence with the dynamics of mean temperatures and climate dryness (Ponomarev & Kharuk, 2016). In the southern Altai, the reduced burned area since 1987 can be attributed to increased moisture and greatly increased investment in fire prevention (Shi et al., 2021). The dynamic changes of fires in the instrumental measurement period driven by human activities and natural processes exhibit distinct differences. However, contemporary observations remain circumscribed by the temporal resolution limitations of satellite archives (post-1980) and instrumental records, creating a <50-year observational window that inadequately captures decadal-scale fire-climate-human feedbacks (Shi et al., 2021; Ponomarev & Kharuk, 2016; Albrich et al., 2018; Kharuk et al., 2021). These both limit our understanding of long-term fire activities in the eological sentivitiy regions.

Paleoecological approaches spanning centennial to millennial timescales provide crucial temporal dimensional support for disentangling the complex interactions through pattern-process analysis. Existing Holocene fire records in the Altai-Sayan ecoregion have established a robust methodological framework for reconstructing fire-vegetation-climate couplings (e.g., Blyakharchuk et al., 2004, 2007, 2008; Hu et al., 2025; Li et al., 2024). However, two critical knowledge gaps remain to be addressed: (1) the complete fire sequence in western Mongolia, and (2) the spatiotemporal linkages between fire in this region and montane ecosystem dynamics across the Altai-Sayan ecoregion. To address this issue, this study selected Achit Nuur as the study site because of its continuous and stable depositional environment. Three critical research dimensions include in this study: (1) Reconstructing fire variability in the Holocene interval (~11.75-0 cal. kyr BP) using high-resolution microscopic charcoal analysis from Achit Nuur; (2) Identifying ecotonal heterogeneity in fire

95 regimes through comparison with other already-published paleofire records (n=23) in

96 the nearby regions; (3) Evaluating how dominant tree genera (*Abies, Betula*, *Larix*,

97 *Picea*, *P. sibirica*, *P. sylvestris*) and their summed percentages as forest cover

98 modulate fire characteristics across vegetation types. This study will clarify the

99 long-timescale fire history in the Altai-Sayan ecoregion, as well as its complex

100 associations with climate fluctuations, vegetation succession and human activities.

101 These outputs provide empirical foundations for developing climate-responsive fire

102 management strategies in the Central Asian ecosystems under the future scenarios.

103 **2. Physiographic Settings**

104 **2.1. The Altai-Sayan Mountains**

105   The Altai-Sayan Mountains, one of the most prominent mountain ranges in

106 Central Asia, connect with the Kazakhstan Hills to the west, border the Southern

107 Siberian Plain to the north, and adjoin the Junggar Basin-Khangai Mountains to the

108 south (Fig. 1; Feng et al., 2017). Climatologically, this region holds great significance,

109 as it likely served as a transitional zone where the Westerlies-dominated climates from

110 the west interacted with the Asian Monsoon-influenced climates from the east during

111 the Holocene (Blyakharchuk et al., 2004, 2008; Zhang & Zhang, 2025). Culturally, it

112 also functioned as a cultural crossroads between Asian and European civilizations

113 along the "Eurasian Steppe Silk Road" (Blyakharchuk & Chernova, 2013; Xiang et al.,

114 2023).

115   The North Atlantic Oscillation and Siberian High drive the southward

116 displacement of the Westerlies, which transport water vapor from the Mediterranean,

117 Caspian, and Black Seas into the study region during winter and spring (Aizen et al.,

118 2001; Kutzbach et al., 2014). In contrast, the interaction between the Asian Low and

119 Azores High regulates the northward shift of the Westerlies, facilitating water vapor

120 transport in summer and autumn (Aizen et al., 2001). These latitudinal shifts of the

121 westerlies induce a southward gradient of decreasing precipitation and increasing

122 climatic aridity, which in turn shapes the characteristic vegetation distribution patterns

123 across the Central Asia (Fig. 1). Zonally, vegetation distribution exhibits a strong

124 latitudinal dependence. Specifically, the coniferous forests dominate the southern

Siberian Plain, while the eastern Kazakhstan Hills and western Mongolia are characterized by steppe ecosystems, and the Junggar Basin is covered by desert-steppe (Chen, 2010). Additionally, the region's vegetation displays distinct vertical zonation with communities transitioning from desert and steppe at lower elevations to forest and alpine meadow at higher elevations (Blyakharchuk & Chernova, 2013; Zhang et al., 2020).

2.2. Achit Nuur

Achit Nuur (49.42°N, 90.52°E; 1444 m a.s.l.) occupies an intermountain basin bounded by the Mongolian Altai to the west, Mungen Taiga Mountain to the north and Kharkhiraa Turgen Mountain to the east (site 1 in Fig. 1) (Sun et al., 2013). The lake exhibits distinct shoreline zonation: low-lying northern/southern margins are salt-marsh vegetation, while the elevated eastern and western shores are dominated by desert steppe communities (Sun et al., 2013). Regional vegetation comprises a mosaic of *Stipa krylovii*, *Stipa gobica* and *Cleistogenes soongorica* grasslands interspersed with subshrubs including *Artemisia frigida*, *A. xerophytica*, *A. caespitosa*, *Tanacetum sibiricum*, *T. achillaeoides* and *T. trifidum*. Mountainous areas of the Mongolian Altai host taiga forests dominated by *Larix sibirica* and *P. sibirica* with an understory of *Rosa acicularis* and *Betula rotundifolia* (Sun et al., 2013).

A 2-m sediment core was retrieved from the central lake basin in 2010 using a Livingston-type piston corer (Sun et al., 2013). Five lithological units were identified based on organic matter (OM) content and mean grain size characteristics (Fig. 2A). Ten bulk samples (Table S1) underwent accelerator mass spectrometry (AMS) ^{14}C dating at the University of Arizona NSF-AMS Facility (Fig. 2A). A 2100-year reservoir correction was applied to all radiocarbon ages prior to calibration due to old carbon-influenced 2099 ^{14}C BP on the surface sediment and this correction is assumed to be constant throughout the whole sequence (Sun et al., 2013). The calibration to calendar years before present (cal. yr BP, relative to 1950 CE) utilized the IntCal20 curve (Reimer et al., 2020). The Bayesian age-depth model was reconstructed using Bacon v2.5.3 (Blaauw & Christen, 2011) (Fig. 2B) and median ages used to calculate the sedimentation rates in yr/cm. It should be pointed out that we analyses the

charcoal data in this study and the pollen and lithology were previously published (Sun et al., 2013). This study just focused on the Holocene interval to investigate the spatial heterogeneities of fire regimes in the Altai-Sayan Mountains and adjacent plains.

2.3. Other study sites in the Altai-Sayan Mountains and adjacent plains

A total of 24 sites, including Achit Nuur (Table 1), were selected to investigate the spatial heterogeneity in fire regimes across the Altai-Sayan Mountains and adjacent plains. These sites were divided into seven regions based on the vegetation distribution and geographic location.

Southeastern/western Altai Mountains within steppe zone (Region A, n=4): Tolbo Lake (site 2; 48.55°N, 90.05°E, 2080 m a.s.l.) is an alpine lake of glacial origin covered by mountain steppe in the Mongolian Altai (Hu et al., 2024). Alahake Lake (site 3; 47.69°N, 87.54°E, 483 m a.s.l.) is located in the Irtysh River valley in the southern Altai Mountains (Li et al., 2019). Kuchuk Lake (site 4; 52.69ºN, 79.84ºE, 98 m a.s.l.) is the largest endorheic basin in Kulunda Basin within the southern Siberia (Rudaya et al., 2020).

Low-relief west Siberian plain (Region B, n=4): Rybnaya Mire (site 5; 57.28ºN, 84.49ºE) is located near the Rybnaya River in the southern taiga of Western Siberia (Feurdean et al., 2022). Plotnikovo Mire (site 6; 56.88ºN, 83.30ºE, 120 m a.s.l) is an ombrotrophic bog located at the eastern margins of the Great Vasyugan Mire in Western Siberia (Feurdean et al., 2020). Shchuchye Lake (site 7; 57.13ºN, 84.61ºE, 80 m a. s. l.) is located in the south taiga zone of the West Siberian plain (Blyakharchuk et al., 2024). Ulukh–Chayakh Mire (site 8; 57.34ºN, 88.32ºE) is located on a terrace of the Chulym river in the southern taiga of Western Siberia (Feurdean et al., 2022).

Northern Altai Mountains (Region C, n=4): Chudnoye Lake (site 9; 54.03ºN, 89.01ºE, 1147 m a.s.l.), Tundra Mire (site 10; 53.79ºN, 88.27ºE, 247 m a.s.l.) and Kuatang Mire (site 12; 51.81ºN, 87.32ºE, 650 m a.s.l.) are located in the northern Altai Mountains in areas covered by wet mountain dark coniferous (with *Abies, P. sibirica* and *Betula*) taiga (Blyakharchuk & Pupysheva, 2022; Blyakharchuk et al., 2024). Mokhovoe Bog (site 11; 52.52ºN, 86.42ºE, 283 m a.s.l.) is located on the

western piedmont of north Altai covered by birch (with *B. pendula+B. pubescens*) and pine (*P. sylvestris*) forest-steppe (Blyakharchuk & Pupysheva, 2022).

Central Altai Mountains within the forest zone (Region D, n=3): Dzhangyskol Lake (site 13; 50.18°N, 87.73°E, 1800 m a.s.l.) is situated in the western Kurai intermontane depression covered with steppe vegetation and bounded by small hills with *P. sibirica* and *L. sibirica* (Blyakharchuk et al., 2008). Two freshwater lakes are situated 1.5-4 km apart at different elevations below the timberline in the Ulagan Plateau: Uzunkol Lake (site 14; 50.48°N, 87.1°E, 1985 m a.s.l.) and Kendegelukol Lake (site 15; 50.50°N, 87.63°E, 2050 m a.s.l.) (Blyakharchuk et al., 2004).

Central Altai Mountains above the forest limit (Region E, n=3): Tashkol Lake (site 16; 50.45°N, 87.67°E, 2150 m a.s.l.) lies at the timberline (upper limit of continuous forest) of Ulagan Plateau in the central part of Russian Altai (Blyakharchuk et al., 2004). Akkol Lake (site 17; 50.25°N 89.62°E, 2204 m a.s.l.) and Grusha Lake (site 18; 50.38°N, 89.42°E, 2413 m a.s.l.) are situated in the western Karginskaya high-mountain depression near the junction of the Chikhachev and Shapshal ranges of the south-eastern part of Russian Altai (Blyakharchuk et al., 2007).

Western Sayan Mountains (2000-2700 m a.s.l.) (Region F, n=3): Buibinskoye Mire (site 19; 52.84°N, 93.52°E, 1377 m a.s.l.) and Bezrybnoye Mire (site 20; 52.81ºN, 93.50ºE, 1395 m a.s.l.) are located in the Yergaki Nature Reserve (Blyakharchuk, 2020). Lugovoe Mire (site 21; 52.85ºN, 93.35ºE, 1299 m a.s.l.) is the largest mire in the Yergaki Natural Park with the largest hydrological catchment in the Western Sayan Mountains (Blyakharchuk and Chernova, 2013).

Khangai Mountains (peaks 4031 m a.s.l.) (Region G, n=3): Three selected sites include Olgi Lake (site 22; 48.32°N, 98.01°E, 2012 m a.s.l.) (Unkelbach et al., 2021), Shireet Naiman Nuur (site 23; 46.53°N, 101.82°E, 2429 m a.s.l.) (Barhoumi et al., 2024) and Ugii Nuur (site 24; 47.77°N, 102.78°E, 1330 m a.s.l.) (Wang et al., 2011).

3. Methods

3.1. Charcoal analysis

The pre-treatment process for charcoal analyses involved the standard pollen extraction method (Tang et al., 2022; Wang et al., 2024). Charcoal particles were

identified using a light microscope, characterized by dark black color, opaque appearance, sharp corners, and straight edges. The treated samples were prepared into pollen slides by adding an appropriate amount of glycerin using the particle counting method, which were then observed and counted under a Lycra microscope. A total of more than 300 particles of all sizes were quantified at 400× magnification using an Olympus BX53 microscope and the quantity of Lycopodium spores was determined for each sample.

The concentration of charcoal was calculated based on the statistical data (Li et al., 2024):

$$W = A * N/(n * N)$$

Where W is the charcoal concentration (particles/g), A is the the total count of charcoal fragments, n is the number of additional lycopodium spores per mount, N is the statistical number of lycopodium spores, and G is the sample weight (g). Charcoal influx (CHAR, particles/cm^2/yr) is calculated by multiplying the concentration dividing by the sedimentation rate (yr/cm) derived from the age-depth model (see paragraph 2.2).

3.2. Generalized additive models

Generalized additive models (GAMs) employ a link function to examine the relationship between the mean of the response variable (i.e., dependent variable) and a smoothed function of the predictor variable (i.e., independent variable). The model convergence and adequacy were assessed using the gam.check() function in R and confirmed that the basis dimensions (k) were sufficient and inspected diagnostic plots of residuals to ensure the model structure was appropriate. In this study, we investigated the associations between charcoal influx and two types of predictors: (1) individual taxa, including *Abies, Betula, Larix, Picea, P. sibirica* and *P. sylvestris,* because they represent the dominant arboreal species in the study area and are key components of the regional forest ecosystems; and (2) total forest cover, defined as the summed percentage of the aforementioned six taxa.

We constructed GAMs with a quasi-Poisson distribution and a log link function using the mgcv package in R (Wood, 2017). This distribution was selected because it

flexibly corrects for overdispersion without requiring a specific parametric distribution for the data (Wood, 2017). For all smoothing terms, we used thin-plate splines as the basis function—this is the default setting in the gam() function of the mgcv package. The model fitting was performed via restricted maximum likelihood (REML) for smoothness selection.

3.3. Data processing for comparison

To render charcoal influx records from different sites comparable, a three-step transformation procedure was applied to calculate comparable Z-scores (Power et al., 2007):

(1) Min-max transformation: Raw influx values were rescaled to a 0-1 range to reduce the influence of varying magnitudes between sites.

$$C_i^{'} = (C_i - C_{min})/(C_{max} - C_{min})$$

In this expression, $C_i^{'}$ is the value of mini-max transformed for the i-th sample at each sequence, C_i is the charcoal influx (CHAR) value for the i-th sample at each sequence, C_{max} is the maximum value of C_i, and C_{min} is the minimum value of C_i.

(2) Box-Cox transformation for homogenization of variance: This transformation was applied to homogenize within-record variance and improve the normality of the data distribution, satisfying the assumptions for subsequent statistical analyses.

$$C_i^* = \begin{cases} ((C_i^{'} + \alpha)^\lambda - 1)/\lambda, \lambda \neq 0 \\ log(C_i^{'} + \alpha), \lambda = 0 \end{cases}$$

In this expression, C_i^* is the Box-Cox value transformed for $C_i^{'}$, λ is the parameter of Box-Cox transformation estimated using maximum likelihood, and α is a small constant added to ensure all data values are positive (>0) prior to the Box-Cox transformation, as the function cannot handle zero values.

(3) Z-score calculation: The transformed data were converted into Z-scores (standardized anomalies with a mean of 0 and unit variance) to facilitate direct comparison and the synthesis of charcoal records across different sites.

$$Z - score = (C_i^* - \overline{C_i^*})/\delta$$

In this expression, $\overline{C_i^*}$ is the average value of C_i^* and δ is the standard deviation

271   of C_i^*.

272   Considering the ~200-year sample resolution at most sites, the transformed

273   Z-scores were linearly interpolated to 200-year time steps. Subsequently, the

274   interpolated data were averaged using a binning method to construct composite curves

275   that characterize fire regimes across different regions. The Holocene interval was

276   divided into three intervals: early Holocene (~11.75-~8.2 cal. kyr BP), middle

277   Holocene (~8.2-~4.2 cal. kyr BP) and late Holocene (~4.2-~0 cal. kyr BP) (Marcott et

278   al., 2013).

279   **4. Results and Discussions**

280   **4.1. Reconstructed fire history and its relationship with vegetation at Achit Nuur**

281   The charcoal influx in Achit Nuur varies from 67 to 2643 particles/cm^2/yr with an

282   average of 501 particles/cm^2/yr. Notably, higher charcoal influx has been recorded

283   since ~2 cal. kyr BP with the maximum occurring during the interval of ~1.2-~0.79

284   cal. kyr BP (Fig. 3a). Regarding pollen trends: *P. sibirica*, *Betula* and *Picea* exhibited

285   a rapid increase before ~6 cal. kyr BP, followed by a gradual decreasing trend (Fig. 3b)

286   (Sun et al., 2013). High *Larix* pollen content was observed from ~6 to ~2 cal. kyr BP,

287   while *Abies* pollen remained relatively low throughout the entire sequence. GAMs

288   analyses reveal charcoal influx is significantly positively correlated with the

289   abundance of *Betula* (Deviance explained=20%, p=0.02), *P. sibirica* (Deviance

290   explained=34.5%, p=0.001) and total forest cover (Deviance explained=41.5%,

291   p<0.001). Conversely, it is significantly negatively correlated with decreasing *Larix*

292   (Deviance explained=41.9%, p<0.001) and *Picea* (Deviance explained=19.2%,

293   p=0.001) abundances (Table 2, Fig. 1).

294   The strong positive relationship between charcoal and forest cover suggests that

295   this region functions as a fuel-limited system, where biomass availability regulates

296   fire activities. Mechanistically, the late-Holocene fire increase coincides with a shift

297   in vegetation composition: the decline of *Larix* (often a fire-avoidant species that

298   maintains moister sub-canopy conditions) after ~2 cal. kyr BP likely increased

299   landscape flammability. In contrast, taxa such as *Betula* and *P. sibirica* possess traits

300   like thinner bark and more resinous tissues (Feurdean et al., 2020, 2022) that facilitate

10

fire spread and intensity. Thus, these shifts in relative species directly regulated the observed variation in charcoal influx.

4.2. Holocene climate-fuel feedbacks across selected sites

4.2.1. Southeastern/western Altai Mountains within the steppe zone (Region A):

Charcoal records from four lacustrine systems (Achit Nuur, Tolbo, Alahake and Kuchuk Lakes) reveal a consistent amplification of fire activity during the late-Holocene (Fig. 4b). Distinct peak intervals vary across sites: ~1.2-~0.79 cal. kyr BP at Achit Nuur, ~1.20-~0.65 cal. kyr BP at Tolbo Lake, ~1.44-~1.02 cal. kyr BP at Alahake Lake, and a pronounced doubling of charcoal flux over the past two millennia at Kuchuk Lake. Pollen spectra highlight the ecosystem-specific fuel configurations that underpin these fire patterns: Tolbo Lake is dominated by an alpine steppe ecosystem (*Artemisia*-Poaceae), where herbaceous plants serve as the primary surface fuel; Achit Nuur features montane *P. sibirica* providing highly flammable resinous fuel sources. Alahake Lake is surrounded by lowland *Picea-Larix* mixed forest, where leaf litter and understory vegetation contribute to fuel loads (Sun et al., 2013; Hu et al., 2024; Li et al., 2019; Rudaya et al., 2020).

This divergence in fuel strategy explains the varied fire responses to environmental changes. GAMs analyses confirm that charcoal influx at Achit Nuur and Tolbo Lake is primarily controlled by forest cover (Table 2, Fig. S1). Specifically, *Larix* (41.9% deviance explained) and *P. sibirica* (34.5%) are key drivers in Achit Nuur, whereas *P. sibirica* (13.3%) plays a dominant role at Tolbo Lake. At Alahake Lake, *Betula* (with its thin bark and volatile leaf litter) is the primary combustion source. Notably, at Kuchuk Lake, the post-2 cal. kyr BP doubling of charcoal influx is explicitly linked to the expansion of *Betula* and *P. sylvestris* forest—both of which possess high ignition potential (Table 2, Fig. S2).

4.2.2. West Siberian plain (Region B, n=4):

Rybnaya Mire, located on the low terrace of the Ob' River (83 m a.s.l.) and dominated by *P. sylvestris* and *Betula*, shows higher influx during the middle Holocene but no significant charcoal pulse over the past 50 years (Feurdean et al., 2020) (Fig. 4c). GAM analysis indicates fire activity is primarily controlled by

coniferous vegetation with *Picea* abundance explaining 44.5% of the variance (Table 2, Fig. S2). In contrast, Plotnikovo Mire exhibits a rapid charcoal increase since ~2 cal. kyr BP (Feurdean et al., 2020). This surge is likely linked to the gradual expansion of *Betula* (forest cover explaining 39.7% of deviance) (Table 2, Fig. S2), as the accumulation of its flammable resinous bark created more favorable conditions for fire ignition and spread (Feurdean et al., 2022). Shchuchye Lake displays a phased fire regime, marked by a strong charcoal pulse at the Younger Dryas-Early Holocene transition (~12-~11 cal. kyr BP) and slightly increased fire activity during the late Holocene (Fig. 4c). Ulukh-Chayakh Mire records key fire events in the last millennium and during the ~4.5-~3 cal. kyr BP interval (Fig. 4c).

GAM analyses reveal the divergent fire-vegetation relationships rooted in canopy structure (Table 2, Fig. S2 and S3): (1) Negative correlation at Rybnaya and Plotnikovo Mires (canopy cover >75%): Dense canopies limit light availability, maintaining humid microclimatic that suppress the herbaceous understory growth. This creates moist surface conditions and sparse fine fuels, resulting in an inverse relationship between canopy cover and fire. (2) Positive correlation at Shchuchye Lake (canopy cover <65%): Open canopy structures allow solar radiation to reach the forest floor, promoting the growth of flammable grassy understories. These fine fuels dry quickly and ignite easily, while the open environment facilitates air circulation and fire spread, leading to a positive association between canopy openness and charcoal influx.

4.2.3. Northern Altai Mountains (Region C, n=4):

Chudnoye Mire, situated in a remote mountain taiga near the upper forest limit (Fig. 1), exhibits a decline in influx during the early to mid-Holocene followed by late Holocene intensification (Fig. 4d). This variations correlates positively with *Betula* (30.3%) and *Picea* (20.5%) abundances (Table 2, Fig. S3). The mechanism lies in pyrophtic properties of these taxa (*Betula* and *Picea*): their needle litter and resinous tissues that are highly flammable when dry, directly boosting fire frequency (Blyakharchuk et al., 2024).

Tundra Mire, characterized by dense forests of *Abies* and *Betula*, shows rising

charcoal influx after ~4 cal. kyr BP. GAM analysis suggests that this trend stems from the fire-adapted traits of *Larix* (22.7% of deviance explained) (Table 2, Fig. S4). Mokhovoe Bog, a birch forest-steppe site, records four charcoal influx peaks at ~11.5–~9.5, ~8.5–~7, ~5.6–~4 and ~1.5–~1 cal. kyr BP. A statistical correlation (11.9%) with *Picea* pollen (Table 2, Fig. S4) suggests a climatic controls on fuel production: humid conditions enhance bioproductivity and litter accumulation. Although *Picea* is less flammable than *Betula*, the sheer increase in fuel loads drives higher charcoal influx (Blyakharchuk, 2022).

Kuatang Lake shows a clear charcoal increase between ~3.5 and ~2 cal. kyr BP (Fig. 4d, Fig. S4). A distinct vegetation-fire pattern emerges here: charcoal influx positively correlated with *Betula* pollen but negatively with *Abies*, *P. sibirica* and *P. sylvestris*. This suggests that the post-3.5 cal. kyr BP fire increase was driven by the expansion of fire-prone *Betula* (thin, volatile bark) at the expense of more fire-resistant conifers (thick bark, dense canopies) (Blyakharchuk et al., 2024).

4.2.4. Central Altai Mountains within the forest zone (Region D, n=3):

Charcoal influx exhibited a consistent increasing trend across Kendegelukol Lake, Uzunkol Lake and Dzhangyskol Lake (Fig. 4e), with pronounced acceleration during the late Holocene. Uzunkol Lake records a sharp rise in charcoal influx since ~1.2 cal. kyr BP, while Dzhangyskol Lake increases markedly from ~0.5 cal. kyr BP onward. Notably, Uzunkol Lake also documented elevated charcoal influx between ~9.5 and ~9 cal. kyr BP, coinciding with the steppe-to-forest transition (Blyakharchuk et al., 2008). This early Holocene peak likely arose from an unstable fire regime during the forest establishment: dry climatic conditions combined with increasing woody fuel loads made the nascent ecosystem highly susceptible to ignition (Blyakharchuk & Pupysheva, 2022). The subsequent landscape stabilization and humidification suppressed fire activity until the late Holocene (Zhang and Zhang, 2025).

Kendegelukol Lake and Dzhangyskol Lake exhibited modest increases in charcoal influx throughout the Holocene (Fig. 4e). This contrast highlights Uzunkol Lake's sensitivity as an ecotone site (Blyakharchuk et al., 2004). Located in the

forest-steppe transition zone, its dynamic vegetation mix is highly responsive to minor climatic fluctuations, amplifying fire signals. In contrast, the cohesive forests at these two sites buffer against small-scale environmental changes (Lezine et al., 2023). GAM analyses across all three lakes reveal strong positive correlations with *Abies*, *Betula* and *P. sylvestris* (Table 2, Fig. S5), confirming that the late-Holocene forest expansion enhanced fuel accumulation, thereby lowering ignition thresholds.

4.2.5. Central Altai Mountains above the forest limit (Region E, n=3):

Tashkol Lake (2150 m a.s.l.) exhits a sharp peak in charcoal influx at ~11-~10.5 cal. kyr BP, likely caused by a paraglacial mechanism: meltwaters redeposition of Pleistocene-aged microcharcoal following deglaciation (Blyakharchuk et al., 2004, 2024). Subsequently, the middle Holocene warming (~10.5-~4 cal. kyr BP) promoted high-elevation expansion, increasing biomass and charcoal influx via a temperature-dependent mechanism. Late Holocene cooling reversed this trend.

Grusha Lake (2413 m a.s.l.) shows a similar pattern with an exceptionally late-glacial (~12-~11 cal. kyr BP) high charcoal influx attributed to the allochthonous redeposition (Rudoy and Yatsuk, 1986; Blyakharchuk et al., 2024). Following deglaciation (~10.5 cal. kyr BP), vegetation colonization stabilized the landscape, shifting the record to reflect in-situ fire activity (Blyakharchuk et al., 2004). Akkol Lake mirrors the general trend but lacks the ~12-~11 cal. kyr BP peak. This absence is explained by its lower elevation and lack of glacial coverage during the last glaciation (Blyakharchuk et al., 2007). Without glaciers to accumulate ancient microcharcoal, and with drier conditions inhibiting sediment transport, Akkol Lake records only minimal in-situ fire activity during this period.

GAMs analyses identify the key vegetation sources of biomass combustion across three lakes: *Picea* (40.7%) in Tashkol Lake; a combination of *Picea* (31.6%) and *Larix* (30.4%) in Akkol Lake; and *Larix* (49.3%) and *Picea* (35.80%) in Grusha Lake (Table 2, Fig. S6). These species-specific associations reflect differences in fuel flammability — *Larix* produce resin-rich needles and bark that ignite easily, while *Picea* litter, though less flammable, contributes to fuel loads when accumulated in

large quantities (Blyakharchuk et al., 2004) — ultimately driving lake-specific variations in charcoal influx. Notably, significant differences in charcoal influx magnitudes and timing were observed among three lakes, largely tied to their distinct elevations, glacial histories and post-glacial vegetation development.

4.2.6. Western Sayan Mountains (Region F, n=3):

Records from Lugovoe Peat, Bezrybnoye Mire and Buibinskoye Mire generally show decreasing Holocene charcoal records. A notable exceptin is the ~12-~11 cal. kyr BP peak at Buibinskoye Mire (Fig. 4g). As permafrost receded and the region transitioned from cold, waterlogged soils supporting sparse *Picea* to better-drained substrates, *P. sibirica* and *Abies* expanded (Blyakharchuk et al., 2013, 2022). The ~11 cal. kyr BP peak reflects this forestation event. A transient warming just prior (~11.5-~11 cal. kyr BP) likely dried sparse spruce litter, triggering intense fires. Following a mid-Holocene maximum (~10.5-~7 cal. kyr BP) driven by warming-enhanced productivity, charcoal influx declined as late-Holocene cooling reduced fuel accumulation.

GAMs results highlight species-specific roles in driving charcoal influx: in Lugovoe Peat, *Abies* and *Larix* are the primary contributor to charcoal production. However, at Bezrybnoye Mire, fire-resistant *P. sylvestris* explains the most variance (28.10%) (Table 2, Fig. S7). This suggests a negative feedback: the expansion of *P. sylvestris* displaced more flammable taxa, reducing overall forest flammability and driving the long-term decline in charcoal influx.

4.2.7. Khangai Mountains (Region G, n=3):

At Olgi Lake, a negative correlation (33.3%) between charcoal influx and primary forest cover suggests fires are fueled by steppe herbs (Table 2, Fig. S8). An decrease in forest cover would promote grass-fueled fires, leading to higher charcoal influx—explaining the observed negative correlation (Sun et al., 2013). Conversely, at Shireet Naiman Nuur (37.4%) and Ugii Nuur (18.4%), positive correlations with forest cover (especially *P. sibirica*) (Table 2, Fig. S8) indicate woody biomass drives fire activity. Despite similar trends, Shireet Naiman Nuur records lower overall influx due to elevation-limited productivity (Barhoumi et al., 2024).

Marked charcoal spikes were recorded at at Olgi Lake (~3.4–~3.1 cal. kyr BP) and Ugii Nuur (~2.4–~2.1 cal. kyr BP), which align with periods of local drought (Unkelbach et al., 2021; Barhoumi et al., 2024; Wang and Feng, 2013). In the absence of significant human impact during these intervals, drought likely acted as a natural catalyst, drying fuels and increasing susceptibility to ignition.

4.3. Holocene climate-fuel feedbacks across the different regions

In Region A, fire activity was suppressed during the dry early Holocene due to limited fuel availability (Zhang and Zhang, 2025; Sun et al., 2013; Hu et al., 2024; Li et al., 2021; Rudaya et al., 2020). From the mid-Holocene to ~2 cal. kyr BP, increased precipitation (Hu et al., 2024; Zhang and Zhang, 2025) facilitated vegetation expansion, fueling a gradual rise in fires. Crucially, after ~2 cal kyr BP, anomalous charcoal peaks across all sites correlate with pollen evidence of agricultural expansion (e.g., cereal-type Poaceae; Xiao et al., 2021). This synchrony suggests that anthropogenic disturbances — specifically intentional burning for pasture and crop management — overrode climatic controls to become the dominant driver of fire frequency (Li et al., 2021; Xiao et al., 2021; Rudaya et al., 2020).

In Region B, fire history divides into three phases: (1) An early pulse (~12-~11 cal. kyr BP) at Shchuchye Lake driven by paraglacial processes (Blyakharchuk et al., 2024); (2) A mid-Holocene increase (~8.5-~6 cal. kyr BP) at Rybnaya Peat linked to the expansion of dark taiga (Feurdean et al., 2022); and (3) A widespread fire surge past ~2 cal. kyr BP. This late-Holocene intensification resulted from the synergistic effects of megadrought conditions (drying vegetation) and the emergence of pastoralist fire use (Feurdean et al., 2022).

In Region C, a late-Holocene increase in fire activity (following an early-Holocene decline) correlates with regional humidification and intensified human occupation (Blyakharchuk et al., 2023; Zhang and Zhang, 2025). While moisture increased biomass, human activities provided ignition sources. Notably, charcoal pulses in the Bronze Age (~4-~3 cal. kyr BP) and Early Iron Age (~3 cal. kyr BP) coincide with metallurgical centers in the Kuznetski Alatau (Slavnin and Sherstova,

1999), linking fire history directly to cultural expansion (Panyushkina, 2012; Agatova et al., 2014; Xiang et al., 2024; Blyakharchuk, 2022;Slavnin and Sherstova, 1999).

In Region D, a 2.3-fold increase in charcoal influx over the last two millennia (Fig. 4e) reflects the cumulative impact of forest expansion (natural fuel buildup) and pastoral burning. The sharp rise after ~1.0 cal kyr BP, in particular, points to intensified land clearance and management by pastoralists, which altered vegetation structure and amplified flammability (Zhang et al., 2022; Blyakharchuk et al., 2004, 2008).

In Regions E and F, long-term trends differ mainly by vegetation trajectory. In Region E, temperature-driven (Blyakharchuk et al., 2007) forest fluctuations dictated fuel loads (Fig. 4f), with a late anthropogenic overprint. In Region F, the progressive expansion of fire-resistant *P. sylvestris* caused a long-term reduction in ecosystem flammability, driving a decline in charcoal influx despite climatic changes (Blyakharchuk et al., 2013, 2022).

In Region G, a disconnect emerges in the late Holocene: despite a humid climate that should support biomass, charcoal influx declined (Unkelbach et al., 2021; Barhoumi et al., 2024). This anomaly is attributed to anthropogenic landscape fragmentation caused by intense grazing (Zhang S.J. et al., 2021). As observed in modern studies, livestock remove fine surface fuels, effectively severing fuel connectivity and suppressing fire spread (Umbanhowar et al., 2009).

Broadly, Holocene fire regimes in the Altai-Sayan Mountains and adjacent plains reflect a shift from climate-limited systems to human-modified systems. Before ~2 cal. kyr BP, fire activity was largely regulated by moisture (limiting fuel in steppe regions A & G) or temperature (limiting fuel in alpine/forest regions E & F). Since ~2 cal. kyr BP, a divergence occurs: in regions with expanding agriculture/pastoralism (A, B, C, D), anthropogenic ignition sources amplified fire activity beyond natural baselines. Conversely, in heavily grazed areas (Region G), pastoral pressure fragmented fuels, suppressing fires. This synthesis highlights the fundamental transition of the Altai-Sayan fire regime from biophysical control to anthropogenic dominance in the late Holocene.

5. Conclusions

This study presents a long-term fire record from western Mongolia and systematically evaluates the spatiotemporal variations in charcoal influx and its coupling with vegetation across the Altai-Sayan Mountains and adjacent plains. Our synthesis reveals distinct regional drivers of fire regimes rooted in climate-fuel feedbacks and, more recently, anthropogenic forcing:

Prior to ~2 cal. kyr BP: Fire activity was primarily regulated by biophysical constraints on fuel availability. In the steppe zone (Region A), low charcoal influx was driven by aridity, which limited vegetation productivity and fuel continuity. In the Central Altai forests (Regions D and E) and Western Sayan (Region F), fire trends generally followed temperature-regulated forest dynamics. Specifically, the early-to-mid Holocene decline in charcoal influx (Regions D, E, and F) reflected shifts in forest composition and cover. Notably, in Region F, this decline was mechanistically linked to the expansion of fire-resistant *P. sylvestris*, which reduced ecosystem flammability by displacing more combustible taxa.

A synchronized surge since ~2 cal. kyr BP in charcoal influx occurred across Regions A, B, C and D. This widespread intensification was driven by the synergistic effects of regional climatic changes and intensified human activities (e.g., agricultural expansion and pastoral burning), which overrode natural fuel limitations. Conversely, Region G exhibited a marked decline in charcoal influx despite favorable climatic conditions. This anomaly is attributed to landscape fragmentation caused by intensive grazing, where livestock pressure reduced surface fuels and suppressed fire spread.

Our findings underscore that fire regimes in the Altai-Sayan ecoregion are determined not just by climate, but by the specific flammability traits of dominant vegetation (e.g., pyrophytic *Betula*/*Larix* vs. fire-resistant *P. sylvestris*) and land-use history. Understanding these long-term fire-vegetation-human interactions provides critical baselines for predicting future wildfire risks and implementing sustainable forest management strategies in a warming world.

CRediT authorship contribution statement

Declaration of Competing Interest

References

Agatova, A.R., Nepop, R.K., Bronnikova, M.A., Slyusarenko, I.Tu., Orlova, L.A. Human occupation of South Eastern Altai highlands (Russia) in the context of Environmental changes. Archaeological and Anthropological Sciences. DOI 10.1007/s12520-014-0202-7.

Aizen, E.M., Aizen, V.B., Melack, J.M., Nakamura, T., Ohta, T., 2001. Precipitation and atmospheric circulation patterns at mid-latitudes of Asia. Int. J. Climatol. 21, 535-556.

Albrich, K., Rammer, W., Thom, D., Seidl, R., 2018. Trade-offs between temporal stability and level of forest ecosystem services provisioning under climate change. Ecological Applications, 28(7), 1884-1896.

Barhoumi, C., Bliedtner, M., Zech, R., Behling, H., 2024. Holocene vegetation, fire, climate dynamics and human impact in the upper Orkhon Valley of the Khangai Mountains, Mongolia. Quat. Sci. Rev. 334, 108713.

Blyakharchuk, T.A., Wright, H.E., Borodavko, P.S., van der Knaap, W.O., Ammann, B., 2004. Late Glacial and Holocene vegetational changes on the Ulagan high-mountain plateau, Altai Mountains, southern Siberia. Palaeogeography,

569   Palaeoclimatology, Palaeoecology, 209(1-4), 259-279.

570   Blyakharchuk, T.A., Wright, H.E., Borodavko, P.S., van der Knaap, W.O., Ammann,
571   B., 2007. Late glacial and Holocene vegetational history of the Altai mountains
572   (southwestern Tuva Republic, Siberia). Palaeogeography, Palaeoclimatology,
573   Palaeoecology, 245(3-4), 518-534.

574   Blyakharchuk, T.A., Wright, H.E., Borodavko, P.S., van der Knaap, W.O., Ammann,
575   B., 2008. The role of pingos in the development of the Dzhangyskol lake-pingo
576   complex, central Altai Mountains, southern Siberia. Palaeogeography,
577   Palaeoclimatology, Palaeoecology, 257(4), 404-420.

578   Blyakharchuk, T.A., Chernova, N.A., 2013. Vegetation and climate in the Western
579   Sayan Mts according to pollen data from Lugovoe Mire as a background for
580   prehistoric cultural change in southern Middle Siberia. Quat. Sci. Rev. 75, 22-42.

581   Blyakharchuk, T.A., Kuryina, I.V., Pologova, N.N., 2019. Late Holocene dynamics of
582   vegetation cover and climate humidity in the southeastern sector of the West
583   Siberian Plain according to palynological and rhizopod studies of peat deposits.
584   Bulletin of Tomsk State University. Biology 45, 164–189. (in Russian)

585   Blyakharchuk, T.A., Pupysheva, M.A., 2022. Indication of fires in the thousand-year
586   history of Central Altai. Geography and Natural Resource, 4, 128-136 (In
587   Russian).

588   Blyakharchuk, T.A., van Hardenbroek, M., Pupysheva, M.A., Kirpotin, S.N.,
589   Blyakharchuk, P.A., 2024. Late Glacial and Holocene history of climate,
590   vegetation landscapes and fires in South Taiga of Western Siberia based on
591   radiocarbon dating and multi-proxy palaeoecological research of sediments from
592   Shchuchye Lake. Radiocarbon, 1-24, doi:10.1017/RDC.2024.103.

593   Blyakharchuk, T.A., 2020. Dynamics of vegetation cover and quantitative
594   palaeoclimatic reconstructions in the Western Sayan Mountains from the Late
595   Glacial period to the present time according to a palynological study of the
596   Yuzhno-Buybinskoe mire. In IOP Conference Series: Earth and Environmental
597   Science (Vol. 611, No. 1, p. 012026). IOP Publishing.

Blaauw, M., Christen, J.A., 2011. Flexible paleoclimate age-depth models using an autoregressive gamma process. Bayesian Analysis 6, 457–474.

Chen, X., 2010. Geography of Chinese Arid Region. Science Press, Beijing (in Chinese).

Feng, Z.D., Sun, A.Z., Abdusalih, N., Ran, M., Kurban, A., Lan, B., Zhang, D.L., Yang, Y., 2017. Vegetation changes and associated climatic changes in the southern Altai Mountains within China during the Holocene. Holocene 27 (5), 683-693.

Feurdean, A., Florescu, G., Tanţău, I., Vannière, B., Diaconu, A. C., Pfeiffer, M., Kirpotin, S., 2020. Recent fire regime in the southern boreal forests of western Siberia is unprecedented in the last five millennia. Quat. Sci. Rev. 244, 106495.

Feurdean, A., Diaconu, A.C., Pfeiffer, M., Gałka, M., Hutchinson, S.M., Butiseaca, G., Gorina, N., Tonlkov, S., Niamir, A., Tantau, I., Zhang, H., Kirpotin S., 2022. Holocene wildfire regimes in Western Siberia: Interaction between peatland moisture conditions and the composition of plant functional types. Climate of the Past 18, 1255–1274

Fu, B.J., Liu, G.H., Ouyang, Z.Y., 2013. Ecological regionalization in China. Beijing: Science Press.

Furyaev, V.V., 1996. Role of Fire in Forest Development. Nauka Publications: Novosibirsk (In Russia).

Ivanova, G.A., Kukavskaya, E.A., Ivanov, V.A., Conard, S.G., McRae, D.J., 2020. Fuel characteristics, loads and consumption in Scots pine forests of central Siberia. J. Forestry Res. 31(6), 2507-2524.

Jones, M.W., Smith, A., Betts, R., Canadell, J.G., Prentice, I.C., Le Quéré, C., 2020. Climate change increases the risk of wildfires. ScienceBrief Rev. 116, 117.

Kasischke, E.S., 2000. Boreal ecosystems in the global carbon cycle. In: Kasischke, E.S., Stocks, B.J. (Eds.), Fire, Climate Change, and Carbon Cycling in the Boreal Forest. Ecological.

Kharuk, V.I., Ponomarev, E.I., Ivanova, G.A., Dvinskaya, M.L., Coogan, S.C., Flannigan, M.D., 2021. Wildfires in the Siberian taiga. Ambio, 50(11), 1953-1974.

629 Kutzbach, J.E., Chen, G., Cheng, H., Edwards, R.L., Liu, Z., 2014. Potential role of
630   winter rainfall in explaining increased moisture in the Mediterranean and Middle
631   East during periods of maximum orbitally-forced insolation seasonality. Clim.
632   Dyn. 42 (3e4), 1079-1095.

633 Goldammer, J.G., Furyaev, V., 2013. Fire in ecosystems of boreal Eurasia (Vol. 48).
634   Springer Science & Business Media.

635 Hu, Y., Huang, X., Demberel, O., et al., 2024. Quantitative reconstruction of
636   precipitation changes in the Mongolian Altai Mountains since 13.7 ka. Catena,
637   234, 107536.

638 Hu, Y., Huang, X., Li, Y., et al., 2025. Holocene fire dynamics in the Altai Mountains
639   and its driving factors. Geophysical Research Letters, 52(9), e2025GL116309.

640 Li, Y., Zhang, Y., Wang, J., Wang, L., Li, Y., Chen, L., Zhao, L., Kong, Z., 2019.
641   Preliminary study on pollen, charcoal records and environmental evolution of
642   Alahake Saline Lake in Xinjiang since 4,700 cal yr BP. Quat. Int. 513, 8–17.

643 Li, Y., Zhang, D., Zhang, Y., Sun, A., Li, X., Huang, X., Zhang, Y., Li, Y., 2024.
644   Distentanging the late-Holocene human–environment interactions in the Altai
645   Mountains within the Arid Central Asia. Palaeogeography, Palaeoclimatology,
646   Palaeoecology, 654, 112466.

647 Liu, F., Liu, H., Xu, C., Shi, L., Zhu, X., Qi, Y., He, W., 2021. Old-growth forests
648   show low canopy resilience to droughts at the southern edge of the taiga. Global
649   Change Biology, 27(11), 2392-2402.

650 Marcott, S.A., Shakun, J.D., Clark, P.U., Mix, A.C., 2013. A reconstruction of
651   regional and global temperature for the past 11,300 years. Science 339,
652   1198-1201.

653 Mo, L., Zohner, C. M., Reich, P. B., Liang, J., De Miguel, S., Nabuurs, G. J., Ortiz-
654   Malavasi, E., 2023. Integrated global assessment of the natural forest carbon
655   potential. Nature, 624(7990), 92-101.

656 Panyushkina, I.P., 2012. Climate-Induced changes in Population Dynamics of
657   Siberian Scythians (700-250 B.C.). Climate, Landscapes and Civilizations.
658   Geographycal Monograph Series 198, 145-154.

659 Ponomarev, E.I., Kharuk, V.I., 2016. Wildfire occurrence in forests of the Altai-Sayan

region under current climate changes. Contemporary Problems of Ecology, 9, 29-36.

Power, M.J., Marlon, J., Ortiz, N., et al., 2007. Changes in fire regimes since the Last Glacial Maximum: an assessment based on a global synthesis and analysis of charcoal data. Climate Dynamics, 30, 887-907.

Reimer, P.J., Austin, W.E., Bard, E., Bayliss, A., Blackwell, P.G., Ramsey, C.B., Talamo, S., 2020. The IntCal20 Northern Hemisphere radiocarbon age calibration curve (0–55 cal kBP). Radiocarbon 62 (4), 725–757.

Rudaya, N., Sergey, K., Michał, S., Xianyong, C., Snezhana, Z., 2020. Postglacial history of the steppe Altai: climate, fire and plant diversity. Quat. Sci. Rev. 249, 106616.

Rudoy, A.N., Yatsuk, T.Yu., 1986. The palaeogeography of southeastern Altai. Chetvertichnaya geologiya i pervobytnaya arkheologiya. Thesis of conference, Ulan-Ude, 73–75.

Shi, C.M., Liang, Y., Gao, C., Wang, Q.H., Shu, L.F., 2020. Drought-modulated boreal forest fire occurrence and linkage with La Nina events in Altai Mountains Northwest China. Atmosphere, 11, 956.

Sun, A., Feng, Z.D., Ran, M., Zhang, C.J., 2013. Pollen-recorded bioclimatic variations of the last ~22,600 years retrieved from Achit Nuur core in the western Mongolian Plateau. Quat. Int. 311, 36-43.

Shi, C.M., Liang, Y., Gao, C., Wang, Q.H., Shu, L.F., 2020. Drought-modulated boreal forest fire occurrence and linkage with La Nina events in Altai Mountains Northwest China. Atmosphere, 11, 956.

Slavnin, V.D., Sherstova L.I. 1999. Aerchaeologic-Ethnographic Essay of Northern Khakassia in the Area of Geological Polygon of Siberian High School). Tomsl Polytechnical University Press, Tomsk (in Russian)

Tang, G., Yang, S., Miao, Y., et al., 2022. Grain size characteristics of microfossil charcoal and the environmental implications in loess deposits from Ganzi, Western Sichuan Plateau. Journal of Lanzhou University (Natural Sciences) 58 (03), 298–305 (in Chinese with English astract).

Umbanhowar Jr, C.E., Shinneman, A.L., Tserenkhand, G., Hammon, E.R., Lor, P.,

Nail, K., 2009. Regional fire history based on charcoal analysis of sediments from nine lakes in western Mongolia. Holocene 19(4), 611-624.

Unkelbach, J., Dulamsuren, C., Klinge, M., Behling, H., 2021. Holocene high-resolution forest-steppe and environmental dynamics in the Tarvagatai Mountains, northcentral Mongolia, over the last 9570 cal yr BP. Quat. Sci. Rev. 266, 107076.

Wang, W., Ma, Y.Z., Feng, Z.D., Narantsetseg, Ts, Liu, K.B., Zhai, X.W., 2011. A prolonged dry mid-Holocene climate revealed by pollen and diatom records from Lake Ugii Nuur in central Mongolia. Quat. Int. 229 (1e2), 74-83.

Wang, Z., Miao, Y., Zhao, Y., Zhang, Z., Zou, Y., Zhang, T., 2024. Preliminary exploration of the fire activity recorded by microcharcoal in surface sediments of Central and Western China. Quat. Sci. 44 (1), 201-213 (in Chinese with English astract).

Wood, S.N., 2017. Generalized Additive Models: An Introduction with R (2nd Edition). Chapman and Hall/CRC, pp1-476.

Xiao, Y., Xiang, L., Huang, X., et al., 2021. Moisture changes in the Northern Xinjiang Basin over the past 2400 years as Documented in Pollen Records of Jili Lake. Front. Earth Sci. 9, 741992.

Xiang, L., Huang, X., Sun, M., Panizzo, V. N., Huang, C., Zheng, M., Chen, F., 2023. Prehistoric population expansion in Central Asia promoted by the Altai Holocene climatic optimum. Nature Communications, 14(1), 3102.

Xinjiang Comprehensive Expedition Team, Institute of Botany, Chinese Academy of Sciences, 1978. Vegetation and its utilization in Xinjiang. Beijing: Science Press.

Zhang, D.L., Feng, Z.D., 2018. Holocene climate variations in the Altai Mountains and the surrounding areas: a synthesis of pollen records. Earth Sci. Rev. 185, 847-869.

Zhang, D., Huang, X., Liu, Q., Chen, X., Feng, Z., 2022. Holocene fire records and their drivers in the westerlies-dominated Central Asia. Sci. Total Environ. 833, 155153.

Zhang, D., Chen, X., Li, Y., Wang, W., Sun, A., Yang, Y., Feng, Z., 2020. Response of vegetation to Holocene evolution of westerlies in the Asian Central Arid Zone.

Quaternary Science Reviews, 229, 106138.

Zhang, S.J., Lu, Y., Wei, W., Qiu, M., Dong, G., Liu, X., 2021. Human activities have altered fire-climate relations in arid Central Asia since ~1000 a BP: evidence from a 4200-year-old sedimentary archive. Sci. Bull. 66(8), 761-764.

Zhang, Y.Y., Zhang, D.L., 2025. Spatiotemporal patterns of pollen-based Holocene precipitation variations in the Altai Mountains and the surrounding areas. Global and Planetary Change, 251, 104832.

Zheng, B., Ciais, P., Chevallier, F., Yang, H., Canadell, J. G., Chen, Y., Zhang, Q., 2023. Record-high CO_2 emissions from boreal fires in 2021. Science, 379(6635), 912-917.
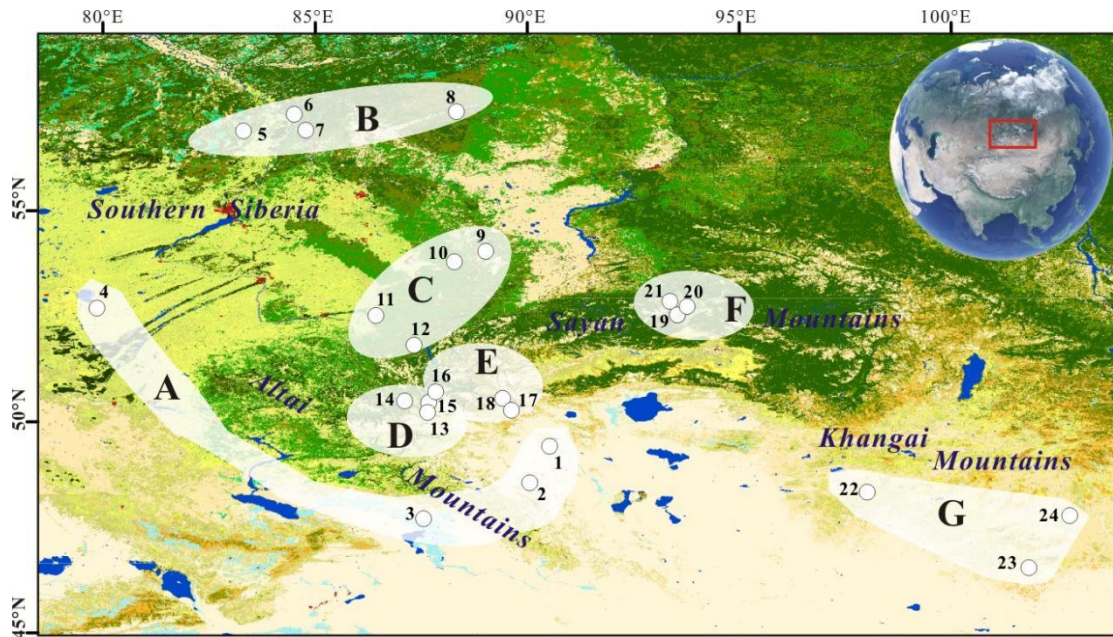
Fig. 1. Spatial distributions of the selected fossil pollen/charcoal sequences across the Altai- Sayan Mountains and adjacent plains. **Region A**: Achit Nuur (1), Tolbo Lake (2), Alahake Lake (3) and Kuchuk Lake (4); **Region B**: Rybnaya Mire (5), Plotnikovo Mire (6), Shchuchye Lake (7) and Ulukh–Chayakh Mire (8); **Region C**: Chudnoye Mire (9), Tundra Mire (10), Mokhovoe Bog (11) and Kuatang Mire (12); **Region D**: Dzhangyskol Lake (13), Uzunkol Lake (14) and Kendegelukol Lake (15); **Region E**: Tashkol Lake (16), Akkol Lake (17) and Grusha Lake (18); **Region F**: Buibinskoye Mire (19), Bezrybnoye Mire (20) and Lugovoe Peat (21); **Region G**: Olgi Lake (OL3) (22), Shireet Naiman Nuur (23) and Uggi Nuur (24).

744
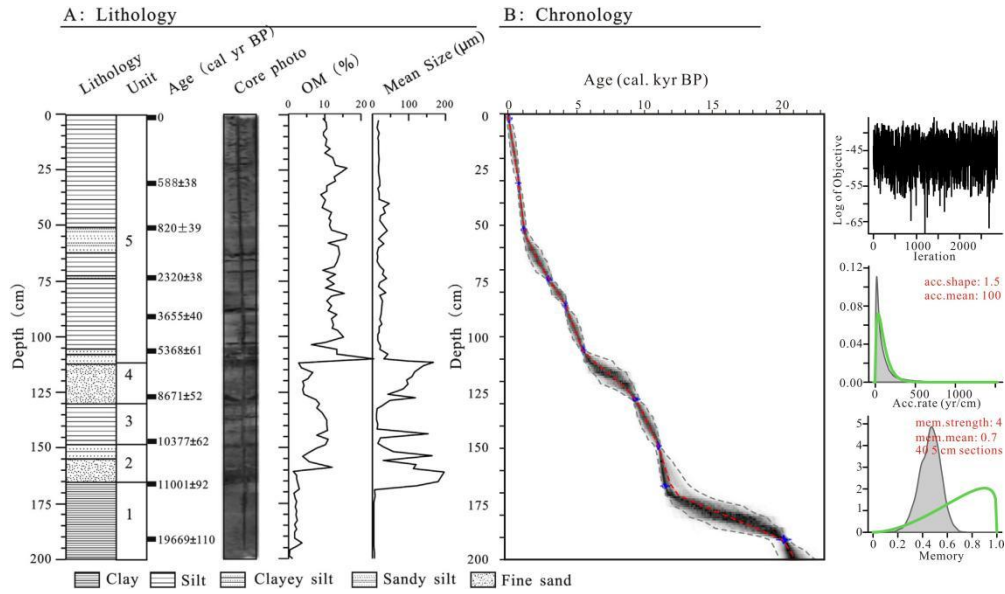
Fig. 2. Lithology, core photo, organic matter (OM), mean grain size and depth-age model in Achit

Nuur (modified from Sun et al., 2023).

747

748

749
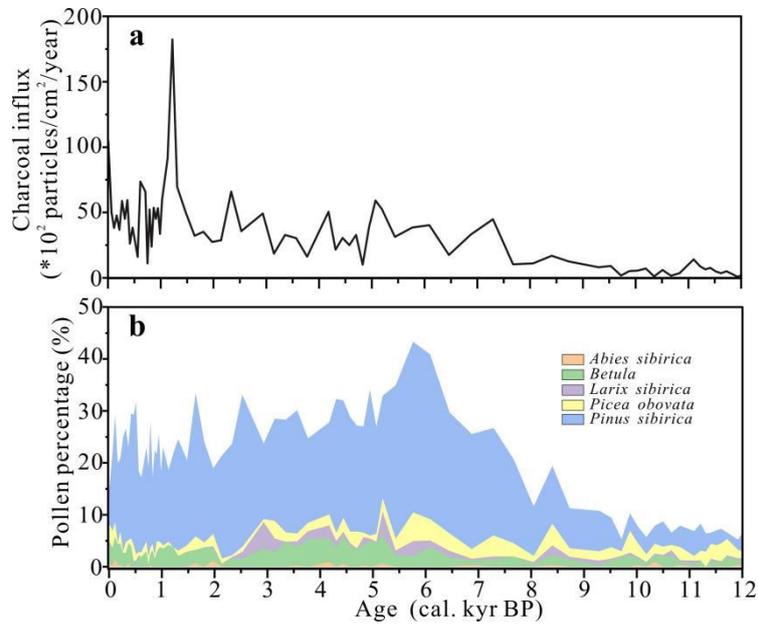
Fig. 3. Achit Nuur: charcoal influx (a) and vegetation change (b) (Sun et al., 2013; this study).
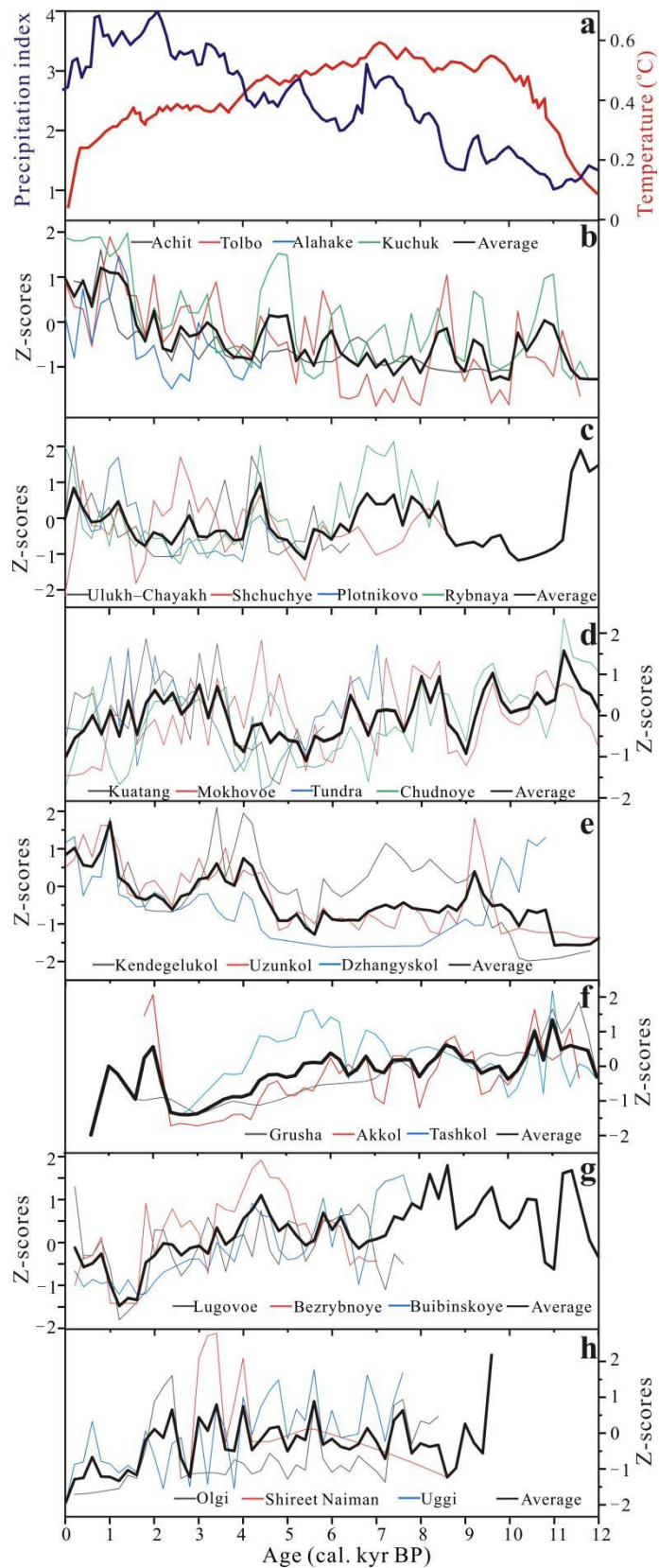
Fig. 4. Regional integrated charcoal influx (b-g) under the context of temperature (Marcott et al., 2013) and precipitation index (a) in the Holocene interval (Zhang and Feng, 2018).

Table 1 Detailed information of the selected sites across the Altai-Sayan Mountains and adjacent plains.

Region	No.	Site Name	Lat. (N)	Long. (E)	Elev. (m a.s.l.)	Core length (cm)	Time interval (cal. kyr BP)	type of charcoal	References
A	1	Achit Nuur	49.42	90.52	1444	200	22.6	micro	this study
	2	Tolbo Lake	48.55	90.05	2080	253	10.3	micro+macro	Hu et al., 2025
	3	Alahake Lake	47.69	87.54	483	140	4.7	micro	Li et al., 2021
	4	Kuchuk Lake	52.69	79.84	98	255	13.1	macro	Rudaya et al., 2020
B	5	Rybnaya Mire	57.28	84.49	-	400	8.4	macro	Feurdean et al., 2022
	6	Plotnikovo Mire	56.88	83.30	120	225	5	macro	Feurdean et al., 2020
	7	Shchuchye Lake	57.13	84.61	80	331	12.8	micro	Blyakharchuk et al., 2024
	8	Ulukh–Chayakh Mire	57.34	88.32	-	348	8.5	macro	Feurdean et al., 2022
C	9	Chudnoye Mire	54.03	89.01	1147	590	12.7	micro	Blyakharchuk et al., 2024
	10	Tundra Mire	53.79	88.27	247	270	7.28	micro	Blyakharchuk et al., 2024
	11	Mokhovoe Bog	52.52	86.42	283	638	16.19	micro	Blyakharchuk, 2022
	12	Kuatang Mire	51.81	87.32	650	557	5.87	micro	Blyakharchuk et al., 2024
D	13	Dzhangyskol Lake	50.18	87.73	1800	380	13	micro	Blyakharchuk et al., 2008
	14	Uzunkol Lake	50.48	87.1	1985	285	12.02	micro	Blyakharchuk et al., 2004
	15	Kendegelukol Lake	50.50	87.63	2050	265	16.01	micro	Blyakharchuk et al.,

29

E	16	Tashkol Lake	50.45	87.67	2150	205	13.57	micro	Blyakharchuk et al., 2004
	17	Akkol Lake	50.25	89.62	2204	470	14	micro	Blyakharchuk et al., 2007
	18	Grusha Lake	50.38	89.42	2413	241	14.37	micro	Blyakharchuk et al., 2007
F	19	Buibinskoye Mire	52.84	93.52	1377	600	13.11	micro	Blyakharchuk et al., 2022
	20	Bezrybnoye Mire	52.81	93.50	1395	600	7.23	micro	Blyakharchuk et al., 2022
	21	Lugovoe Peat	52.85	93.35	1299	330	7.74	micro	Blyakharchuk et al., 2013
G	22	Olgi Lake(OL3)	48.32	98.01	2012	235	9.57	micro	Unkelbach et al., 2021
	23	Shireet Naiman Nuur	46.53	101.82	2429	178	7.4	micro	Barhoumi et al., 2024
	24	Uggi Nuur	47.77	102.78	1330	200	22.6	micro	Wang et al., 2011

757

758

759

Table 2 Correlation between the independent variables represented by pollen percentages (*Abies, Betula*, *Larix*, *Picea*, *Pinus sibirica*, *Pinus sylvestris* and their sum (i.e., forest cover) and the dependent variable (charcoal influx). The significance of each parameter is given by p values where ***p < 0.001; **p < 0.01; *p < 0.05.

Site Name	Independent variable	edf	ref.df	F value	p-value	Deviance explained
Achit Nuur	*Abies*	-	-	-	-	-
	Betula	2.75	3.47	3.40	0.02*	21%
	Larix	3.51	4.21	8.72	0.00***	41.9%
	Picea	1	1	11.36	0.001**	19.2%
	Pinus sibirica	2.73	3.41	5.70	0.001**	34.5%
	Pinus sylvestris	-	-	-	-	-
	Forest cover	2.92	3.69	8.02	0.00***	41.5%
Tolbo Lake	*Abies*	-	-	-	-	-
	Betula	6.96	8.01	1.76	0.09	7.04%
	Larix	1.03	1.07	0.03	0.95	0.03%
	Picea	2.97	3.75	4.47	0.002**	8.11%
	Pinus sibirica	2.68	3.39	9.55	0.00***	13.3%
	Pinus sylvestris	-	-	-	-	-
	Forest cover	2.98	3.75	8.96	0.00***	14.3%
Alahake Lake	*Abies*	1	1	0.57	0.45	1.1%
	Betula	1	1	4.19	0.04*	5.2%
	Larix	6.85	7.94	1.42	0.19	11.6%
	Picea	3.84	4.77	1.96	0.09	10%
	Pinus sibirica	5.59	6.77	1.85	0.09	13%
	Pinus sylvestris	-	-	-	-	-
	Forest cover	2.17	2.77	1.24	0.26	5.07%
Kuchuk Lake	*Abies*	1.21	1.40	3.80	0.03*	9.81%
	Betula	1.38	1.67	16.18	0.00***	25.2%
	Larix	1.11	1.21	0.01	0.98	0.19%
	Picea	1.16	1.30	1.31	0.30	2.29%
	Pinus sibirica	5.84	6.89	1.06	0.39	9.51%
	Pinus sylvestris	6.54	7.64	2.61	0.01*	25.5%
	Forest cover	3.59	4.47	1.22	0.28	11%
Rybnaya Mire	*Abies*	5.28	6.31	1.99	0.07	11.7%
	Betula	4.90	6.00	3.32	0.004**	18.4%
	Larix	7.07	8.11	1.95	0.07	20.6%
	Picea	8.15	8.79	14.1	0.00***	44.5%
	Pinus sibirica	6.74	7.86	1.68	0.12	16.6%
	Pinus sylvestris	2.03	2.54	1.06	0.35	4%
	Forest cover	7.00	8.10	3.06	0.003**	16.2%
Plotnikovo	*Abies*	3.12	3.88	0.70	0.55	16.7%

Mire	*Betula*	2.69	3.36	1.40	0.26	19.6%
	Larix	1	1	4.09	0.06	20.1%
	Picea	2.12	2.65	1.54	0.26	15.1%
	Pinus sibirica	1.68	2.11	0.41	0.7	4.85%
	Pinus sylvestris	2.01	2.53	1.50	0.23	14.7%
	Forest cover	4.43	5.21	4.07	0.004**	39.7%
Schuchye Lake	*Abies*	4.78	5.85	5.39	0.00***	37.4%
	Betula	1	1	5.29	0.03*	10.8%
	Larix	1	1	63.71	0.00***	45.4%
	Picea	2.19	2.71	3.77	0.02*	17.5%
	Pinus sibirica	1	1	27.6	0.00***	30.8%
	Pinus sylvestris	3.15	3.90	3.31	0.02*	21.2%
	Forest cover	2.10	2.52	7.91	0.00***	24.7%
Ulukh–Chay akh Mire	*Abies*	6.38	7.52	1.60	0.18	29.4%
	Betula	1	1	6.44	0.01*	13.4%
	Larix	2.54	3.16	2.46	0.07	17.5%
	Picea	2.45	3.12	1.46	0.23	16.7%
	Pinus sibirica	1	1	0.66	0.42	1.82%
	Pinus sylvestris	1	1	4.43	0.04*	10.3%
	Forest cover	4.26	5.08	1.46	0.22	16.9%
Chudnoye Lake	*Abies*	1.75	2.17	2.09	0.14	8.52%
	Betula	1.23	1.42	10.54	0.001**	23.5%
	Larix	2.06	2.57	3.84	0.03*	14.7%
	Picea	1.99	2.44	11.76	0.00***	30.3%
	Pinus sibirica	4.33	5.25	3.38	0.01*	26.6%
	Pinus sylvestris	1	1	6.59	0.01*	11.6%
	Forest cover	1	1	1.97	0.17	3.5%
Tundra Mire	*Abies*	2.16	2.75	0.78	0.57	3.83%
	Betula	1	1	3.27	0.07	4.44%
	Larix	6.41	7.35	4.32	0.00***	22.7%
	Picea	1	1	0.09	0.77	0.13%
	Pinus sibirica	2.39	2.99	0.83	0.46	4.66%
	Pinus sylvestris	3.03	3.78	0.79	0.49	5.83%
	Forest cover	1	1	2.79	0.10	3.53%
Mokhove Bog	*Abies*	1.83	2.31	1.12	0.38	3.65%
	Betula	6.81	7.88	2.07	0.05	17.2%
	Larix	1.09	1.17	0.24	0.63	0.59%
	Picea	2.59	3.22	3.54	0.02*	11.9%
	Pinus sibirica	1	1	0.00	0.96	0.003%
	Pinus sylvestris	4.46	5.49	1.78	0.11	13%
	Forest cover	5.04	6.19	0.91	0.48	10.3%
Kuatang Mire	*Abies*	2.45	3.14	2.78	0.04*	13.8%
	Betula	1	1	29.13	0.00***	24.5%

_____	Larix	1	1.00	0.06	0.81	0.08%
	Picea	6.72	7.79	1.19	0.31	13.4%
	Pinus sibirica	1.43	1.74	2.92	0.05*	6.90%
	Pinus sylvestris	1	1	5.83	0.02*	6.51%
	Forest cover	1	1	9.24	0.003**	10.9%
Dzhangyskol Lake	Abies	3.64	4.53	0.45	0.79	16.9%
	Betula	1.79	2.23	0.37	0.77	7.12%
	Larix	1	1	0.05	0.83	0.33%
	Picea	3.92	4.80	0.82	0.51	24.8%
	Pinus sibirica	1.70	2.12	0.35	0.73	7.06%
	Pinus sylvestris	3.05	3.75	1.22	0.29	22.8%
	Forest cover	2.39	3.04	0.67	0.58	15.6%
Uzunkol Lake	Abies	1	1	5.329	0.02*	7.04%
	Betula	4.92	5.99	3.22	0.01**	29.4%
	Larix	1	1	14.38	0.00***	22.1%
	Picea	5.99	7.12	5.03	0.00***	40.1%
	Pinus sibirica	2.04	2.57	1.99	0.14	14.7%
	Pinus sylvestris	4.79	5.81	2.85	0.02*	29.3%
	Forest cover	2.17	2.69	1.39	0.27	14.2%
Kendegelukol Lake	Abies	4.93	5.97	2.63	0.04*	41.4%
	Betula	5.87	7.04	2.78	0.02*	49.4%
	Larix	1	1	3.11	0.09	9.63%
	Picea	2.99	3.73	2.19	0.08	29.4%
	Pinus sibirica	2.25	2.78	2.26	0.09	28.9%
	Pinus sylvestris	1	1	18.48	0.00***	40%
	Forest cover	1.57	1.91	3.58	0.06	26.9%
Tashkol Lake	Abies	1	1	0.02	0.90	0.09%
	Betula	1	1	0.08	0.79	0.36%
	Larix	1.56	1.92	0.20	0.82	3.52%
	Picea	6.69	7.81	2.35	0.04*	40.7%
	Pinus sibirica	1	1	0.004	0.95	0.02%
	Pinus sylvestris	1	1	0.02	0.89	0.09%
	Forest cover	3.00	3.75	0.90	0.48	17%
Akkol Lake	Abies	1.76	2.11	0.79	0.43	4.83%
	Betula	1	1	0.96	0.33	1.76%
	Larix	6.53	7.59	1.94	0.08	30.4%
	Picea	2.41	3.03	6.77	0.00***	31.6%
	Pinus sibirica	4.35	5.41	1.90	0.1	23%
	Pinus sylvestris	1	1	10.12	0.002**	18.9%
	Forest cover	8.47	8.92	5.49	0.00***	55.1%
Grusha Lake	Abies	1	1	0.62	0.44	2.75%
	Betula	1	1	0.88	0.36	3.93%

	Larix	3.81	4.58	3.44	0.02*	49.3%
	Picea	2.18	2.71	3.30	0.05*	35.80%
	Pinus sibirica	1	1	0.60	0.45	2.67%
	Pinus sylvestris	1.39	1.66	0.19	0.76	4.67%
	Forest cover	2.55	3.18	12.7	0.00***	71.1%
	Abies	1.15	1.29	0.31	0.75	1.16%
	Betula	1.74	2.20	1.63	0.22	8.85%
Bezrybnoe Mire	*Larix*	2.58	3.14	0.32	0.79	4.76%
	Picea	1	1	2.13	0.15	4.49%
	Pinus sibirica	1.37	1.66	0.39	0.75	2.18%
	Pinus sylvestris	6.47	7.53	1.69	0.13	28.1%
	Forest cover	1	1	0.01	0.93	0.02%
	Abies	2.71	3.39	4.85	0.004**	29.6%
	Betula	2.11	2.69	2.29	0.10	17.4%
Buibinskoye Mire	*Larix*	1	1	1.16	0.29	2.83%
	Picea	1.52	1.87	0.71	0.40	4.85%
	Pinus sibirica	2.02	2.57	2.70	0.05	17.4%
	Pinus sylvestris	1	1	3.78	0.06	7.42%
	Forest cover	3.61	4.42	2.47	0.06	22.6%
	Abies	1	1	6.32	0.02*	15.3%
	Betula	1	1	0.23	0.64	0.79%
Lugovoe Mire	*Larix*	5.00	5.91	3.89	0.01**	43.5%
	Picea	4.00	4.95	2.41	0.07	35.8%
	Pinus sibirica	3.43	4.28	2.20	0.09	31%
	Pinus sylvestris	8.81	8.98	3.21	0.01*	60.5%
	Forest cover	1.14	1.27	0.20	0.67	2.29%
	Abies	-	-	-	-	-
	Betula	4.89	5.96	2.91	0.02*	34.5%
	Larix	4.32	5.29	2.68	0.03*	35.6%
Olgi Lake	*Picea*	3.8	4.65	4.20	0.003**	35.7%
	Pinus sibirica	8.62	8.89	45.23	0.00***	27.9%
	Pinus sylvestris	-	-	-	-	-
	Forest cover	1.74	2.21	7.46	0.00***	33.3%
	Abies	-	-	-	-	-
	Betula	2.57	3.211	3.82	0.01*	20.7%
	Larix	1	1	1.59	0.21	2.83%
Shireet Naiman Nuur	*Picea*	1	1	6.55	0.01*	9.70%
	Pinus sibirica	3.98	4.91	4.02	0.003**	27.5%
	Pinus sylvestris	1	1	7.99	0.01**	12%
	Forest cover	4.01	4.96	6.38	0.00***	37.4%
	Abies	-	-	-	-	-
Uggi Nuur	*Betula*	6.49	7.59	2.02	0.06	8.65%
	Larix	6.48	0.06	104.4	0.00***	12.2%

Picea	1	1	0.18	0.67	0.1%
Pinus sibirica	8.55	8.94	6.19	0.00***	19.4%
Pinus sylvestris	-	-	-	-	-
Forest cover	8.07	8.76	5.72	0.00***	18.4%

764

765